Journal of Materials Chemistry B

ROYAL SOCIETY OF CHEMISTRY

PAPER

View Article Online
View Journal | View Issue

Cite this: J. Mater. Chem. B, 2026, 14, 2644

Poly(D,L-lactide)-grafted Cu-doped bioactive glass microspheres as core–shell building blocks for biomaterials: from grafting to early-stage *in vitro* behaviour

Gabriele Vecchio,[ab] Valentine Poissonnet,[bc] Audrey Béthry,[a] Marie-Pierre Castanié-Cornet,[d] Agnès Dupret-Bories,[bc] Christèle Combes,[b] Fabien Brouillet,[b] Sylvain Le Grill,[b] David Bertrand,[b] Vincent Darcos[a] and Jérémy Soulié*[b]

Received 10th October 2025,
Accepted 21st January 2026

DOI: 10.1039/d5tb02273h

rsc.li/materials-b

Freeze-casting enables the fabrication of porous scaffolds for bone reconstruction, but the homogeneous dispersion of bioactive glass (BG) in polymer solutions remains challenging. Here, we report, for the first time, the synthesis of core–shell microparticles combining Cu-doped BG with poly(D,L-lactide) (PDLLA) grafted *via* a surface-initiated "grafting from" approach. Covalent grafting was confirmed by FT-IR spectroscopy and TGA analyses, with grafted chain lengths close to theoretical values. In simulated body fluid (SBF), the PDLLA corona temporarily delayed glass degradation and ion release, mitigating the initial "burst effect", particularly for Cu^{2+}. *In vitro*, all samples displayed dose-dependent antibacterial and cytotoxic responses, but PDLLA-grafted particles improved cell viability while preserving antibacterial activity. Notably, PDLLA-BG5 achieved the best balance between bacterial inhibition and cytocompatibility. These polymer-grafted, Cu-doped BG microspheres represent promising candidates as building blocks for future PDLLA-based scaffold fabrication *via* freeze-casting approaches, with scalable processing and tuneable ion-release-driven biological responses.

1. Introduction

The demand for bone substitutes in maxillofacial surgery is increasing with the development of synthetic biomedical implants tailored to defect size and patient's pathological condition.[1,2] For critical-size defects, such scaffolds must exhibit optimal macroporosity and appropriate properties to support cell adhesion and proliferation, angiogenesis, and bone formation, thereby ensuring implant osteointegration.[3–5] In some cases, additional features are also required, such as antibacterial activity, particularly in infection-associated pathologies like mandibular osteoradionecrosis (MORN).[6,7] Bioactive glasses are promising bone substitute materials due to their strong osteointegration potential.[8–11] Upon contact with biological fluids, they degrade, releasing active ions (SiO_4^{4-}, Ca^{2+}, PO_4^{3-}) that stimulate bone reconstruction and form a hydroxyapatite layer, enhancing implant-bone bonding.[12,13] Incorporation of metallic ions further improves biological activity, *e.g.*, Cu^{2+} doping promotes angiogenic, osteogenic, and antibacterial properties,[14–20] useful in conditions such as MORN. To overcome brittleness, bioactive glasses are often combined with biodegradable polymers, notably poly(D,L-lactide), which provides biocompatibility, mechanical strength, and ductility for porous scaffolds.[21–26]

Several methods exist for fabricating polymer-based porous scaffolds, including electrospinning,[27,28] solvent casting[29,30] and freeze-drying,[31] all dependent on solvent selection.[29,32–36] Freeze-casting, based on solvent solidification and sublimation, yields oriented porous structures and can process many composites if components disperse well and segregate from solvent crystals.[33,34] In polyester/bioactive glass systems, uniform filler distribution is crucial for consistent mechanical and biological properties.[35] Colloidal stability of hydrophilic inorganic particles in organic solvents (such as dimethyl carbonate) is key, yet combining biodegradable polyesters with bare bioactive glass remains challenging due to poor polymer-filler-solvent affinity, causing aggregation and inhomogeneity.[10,21,28,37–41] Covalent grafting of polymer chains onto the surface of bioactive glass particles can effectively overcome this limitation. This method, commonly referred to as the "bricks and mortar" approach,[42] enhances dispersibility through the synergy of

[a] Department of Polymers for Health and Biomaterials, IBMM, Univ Montpellier, CNRS, ENSCM, 34090 Montpellier, France
[b] CIRIMAT, Toulouse INP, Université de Toulouse, CNRS, ENSIACET, 31030 Toulouse, France. E-mail: jeremy.soulie@toulouse-inp.fr
[c] Otolaryngology, Head and Neck Surgery Department, University Cancer Institute Toulouse and Toulouse University Hospital, Larrey Hospital, Toulouse, France
[d] Laboratoire de Microbiologie et Génétique Moléculaires, Centre de Biologie Intégrative, Université de Toulouse, CNRS, UPS, Toulouse, France

favourable enthalpic interactions (grafted chains/solvent) and steric interactions among the grafted particles themselves.[43] Accurate determination of the grafted polymer properties (M_n, $Đ$, DP, *i.e.* average molecular weight, dispersity and degree of polymerisation), as well as grafting density and inorganic particle characteristics (specific surface area, size, morphology), is essential to properly understand the behaviour of hybrid particles in solution, yet their characterisation remains a challenge.

Two main strategies exist for synthesising polymer-grafted particles: ''grafting onto'' and ''grafting from'' In the former, functionalised particles are coupled with preformed polymers bearing complementary groups, allowing prior characterisation of both components (nuclear magnetic resonance (NMR), size exclusion chromatography (SEC), transmission electron microscopy (TEM) *etc.*). Biodegradable polyesters, such as poly(D,L-lactic acid) (PDLLA), have been successfully grafted onto amino-functionalised silica nanoparticles (NPs) for nanocomposites involved in biomedical applications.[44–47] However, this method is limited by low grafting density due to steric hindrance from pre-attached chains.[45]

The ''grafting from'' approach relies on surface-initiated polymerisation, where monomers grow directly from functional groups on particle surfaces acting as macroinitiators. Techniques such as atom transfer radical polymerisation (ATRP),[48,49] reversible addiction-fragmentation chain transfer polymerisation (RAFT),[50] and ring opening polymerisation (ROP)[51] yield higher grafting densities and molecular weights than the ''grafting onto'' method,[52,53] though propagation control is limited by steric hindrance of immobilized chains. Once core–shell structures are formed, polymer characterisation requires indirect methods such as chain cleavage, free initiator addition, or thermogravimetric analysis (TGA).[54–56] This strategy has enabled the synthesis of highly grafted, well-dispersed silica and bioactive glass nanoparticles with biodegradable polyesters, notably *via* ROP of ε-caprolactone, L-lactide, and D,L-lactide.[53,58–62]

Despite the strong potential of the ''grafting from'' strategy, it has so far only been applied to nanoscale bioactive glass particles obtained through Stöber-derived syntheses.[57] While these nanoparticles are of particular interest, their production *via* sol–gel chemistry involves large quantities of flammable solvents such as ethanol and results in low yields and highly agglomerated nanospheres, making them unsuitable for the large-scale fabrication of implantable scaffolds. To address this limitation and, as an alternative to copper-doped nanoparticles,[58,59] we have recently developed[60] the first synthesis of Cu-doped ternary bioactive glass microparticles (MPs) by combining spray-drying and sol–gel chemistry. Although this method offers far better industrial scalability, the resulting microparticles (due to their larger size and mass) are more prone to sedimentation especially in organic solvent adapted for polyesters. Therefore, their functionalisation, particularly with long polymer chains, is essential. To the best of our knowledge, the ''grafting from'' approach has never been applied to such microparticles. Its implementation presents several challenges, especially due to their lower specific surface areas and larger radii of curvature compared to nanoparticles. Beyond the synthesis itself, the effect of a grafted polyester corona (regardless of the grafting method) on the acellular degradation mechanisms of bioactive glass particles and the *in vitro* properties (such as cytocompatibility and antibacterial properties) has yet to be explored.

In response to these challenges, the present research work aims to report the synthesis of poly(D,L-lactide)-grafted bioactive glass microparticles *via* ''grafting from'' approach. The microparticles selected for grafting are Cu-doped ternary bioactive glass particles (with Cu contents of 0, 1, 2.5, and 5 at%) synthesised *via* spray-drying technique and previously reported in our earlier work.[60] This study will first focus on the surface-initiated ROP of D,L-lactide from the surface of these spray-dried microspheres. The resulting core–shell particles will be characterised in terms of their morphology, physicochemical properties and grafting density using a range of analytical techniques. The second part will assess the acellular reactivity of these core–shell structures in simulated body fluid (SBF), specifically investigating morphological, compositional, and structural changes, as well as ion release profiles. These results will be compared with those of the non-grafted microspheres, with particular attention to copper release kinetics and influence of the PDLLA corona. Finally, this comparative approach will be extended to evaluate the *in vitro* behaviour of these microspheres (particularly their antibacterial activity and cytocompatibility) and to correlate these biological responses with the previously established physicochemical characteristics.

2. Materials and methods

2.1. Raw materials

3-(Aminopropyl)triethoxysilane (APTES, 99%), tin(II) 2-ethylhexanoate ($Sn(Oct)_2$; 92.5–100.0%) and ethyl acetate (puriss. p.a., ACS reagent, ≥99.5% (GC)) were purchased from Sigma-Aldrich, while anhydrous toluene (ERBAdry®) was provided by Carlo Erba. All these reagents were used without further purification. D,L-Lactide (racemic mixture) was obtained from Corbion Purac (PURASORB® DL). Triethylamine (TEA, ≥99.9%) was provided by Sigma-Aldrich and distilled over molecular sieves before use.

All the reactants involved in the preparation of simulated body fluid (SBF) solution, sodium chloride (NaCl, ≥98%), potassium chloride (KCl, 99.5–101.0%), magnesium chloride hexahydrate ($MgCl_2{\cdot}6H_2O$, 99.0–101.1%), calcium chloride dihydrate ($CaCl_2{\cdot}2H_2O$, 99.0–103.0%), di-potassium hydrogen phosphate trihydrate ($K_2HPO_4{\cdot}3H_2O$, ≥99%), sodium sulphate anhydrous (Na_2SO_4, 98.5–101.0%), tris-(hydroxymethyl) aminomethane (TRIS, ≥99%) and sodium hydrogen carbonate ($NaHCO_3$, 100.1%) were of analytical grade and provided by VWR chemicals. All the chemicals were used as received, without further purification. Ultrapure water (ρ = 18.2 MΩ cm) was obtained through Millipore Milli-Q water system.

2.2. Synthesis of core–shell bioactive glass microspheres

2.2.1. Synthesis of Cu-doped ternary bioactive glass microspheres by spray-drying. Cu-doped bioglass (BG) microspheres

with composition SiO_2–CaO–P_2O_5–CuO were synthesised by coupling the sol–gel method and the spray-drying process. Four compositions of MPs, each with varying Cu content, were obtained by substituting copper for the Ca cations. The nominal compositions were 67.5SiO_2, $(25 - x)$CaO, 7.5P_2O_5, (x)CuO (at%), where x = 0, 1, 2.5, 5 at% and respectively denominated BG0, BG1, BG2.5 and BG5. The procedure to obtain these microspheres was already illustrated in our previous research work.[60]

2.2.2. Amino-functionalisation of the spray-dried microspheres. The amino-functionalisation procedure was taken from the work of Lagarrigue *et al.*[44] In the typical amino-functionalisation synthesis of b-BG MPs, 8 g of MPs were dispersed in 320 mL of anhydrous toluene in a three-neck round-bottom flask by means of ultrasound bath and magnetic stirring for 20 minutes. After that, the flask was sealed and equipped with a condenser and placed in an oil bath at 80 °C. The suspension of MPs was degassed by bubbling nitrogen for 15 minutes. 80 mL of APTES were picked up under inert atmosphere, then it was injected in the reaction flask while maintaining a constant nitrogen flux, which was removed just after the beginning of the reaction. Thus, the solution was refluxed overnight under magnetic agitation. Once the reaction was completed, the functionalised MPs were separated from the medium by centrifugation (5000 rpm, 10 min) into proper Teflon (TEP) tubes. In order to remove the unreacted APTES, the resulting powder underwent two additional redispersion/centrifugation cycles (5000 rpm, 5 min), by redispersing the particles into 40 mL of anhydrous toluene at each cycle. Finally, the powder was collected and dried *in vacuo* at 70 °C for 24 hours. The four MPs samples will be labelled as NH_2-BGx.

2.2.3. Surface-initiated ring opening polymerisation of D,L-lactide for the surface of amino-functionalised microspheres. The surface-initiated ROP of D,L-lactide was carried out through the standard Schlenk technique in solution by using the amino-functionalised MPs as macroinitiator. All the four polymerisations were performed by taking a MPs/D,L-lactide mass ratio equal to 0.2 wt wt^{-1}, since the grafting density of primary amines on the NH_2-BGx surface was determined in a second moment through TGA analysis. In the synthesis of PDLLA-functionalised particles, 10 g of NH_2-BGx, which correspond to 1.29 mmol of primary amines (ρ_{NH_2} = 0.129 mmol g_{MPs}^{-1}) were previously dried under vacuum at 80 °C overnight. Then, the powder was dispersed in anhydrous toluene (70 mL) into a dried Schlenk tube by means of an ultrasound microtip (18 W, 10 min) directly immersed in the medium. After that time, 40 g of D,L-lactide (0.277 mol, [D,L LA] = 4 M) were added to the suspension and the Schlenk was put under magnetic stirring, sealed with a rubber septum and solution was degassed by bubbling nitrogen for further 10 minutes. Stannous octoate (0.26 mmol) and triethyl amine (0.65 mmol) were subsequently injected through the septum, so the Schlenk was immersed in an oil bath at 100 °C under a constant nitrogen pressure and continuous agitation for 24 hours. The monomer conversion was monitored by ^{1}H NMR analysis of samples taken up directly from the reaction mixture. The spectra of the crude products at the end of the ROP are reported in Fig. S3. The resulting suspension contained polymer-grafted microparticles (denominated PDLLA-BGx) and free polymer chains probably initiated by residual moisture or other polar compounds. In order to separate the free polymer chains and recover only PDLLA-BGx, the resulting suspension was precipitated into cold ethyl acetate (700 mL), which is a good solvent for both D,L-lactide and free PDLLA chains. The core–shell particles were then recovered by centrifugation in TEP tubes (5000 rpm, 5 min), and the resulting powder underwent two additional redispersion/centrifugation cycles by dispersing the particles in 70 mL of ethyl acetate. Finally, the purified powder was dried under vacuum to remove the traces of solvent. The supernatant solution derived from the four PDLLA-BGx samples purification was collected, concentrated and dried under vacuum, so that the free PDLLA chains could be analysed by size exclusion chromatography (SEC) analysis.

2.3. Characterisation of core–shell bioactive glass/PDLLA microspheres

2.3.1. Morphological, physico-chemical analysis and ion release profiles. Particle's morphology was observed by scanning electron microscopy (SEM) with a FEI Quanta450 in low vacuum mode (water vapor pressure: 90 Pa). Images were registered in secondary electron mode (SE), with a working distance around 10 mm and an accelerating voltage of 12.5 kV. Samples were sputtered with silver plasma for 3 min prior to be examined, using a Scancoat 6 Sputter Coater. SEM-Energy-dispersive X-ray spectroscopy (EDX) was also carried out in order to determine the particles elemental composition. Samples were compressed into pellets and fixed on the SEM supports by means of a carbon adhesive strip. Average molecular weights (M_n) and dispersity ($Đ$) of the free PDLLA chains were determined using size exclusion chromatography (SEC) on a Shimadzu Prominence system (Shimadzu Corp, Kyoto, Japan). The system was equipped with a PLgel MIXED-C guard column (Agilent, 5 μm, 50 × 7.5 mm), two mixed medium columns PLgel MIXED-C (5 μm, 300 × 7.8 mm), and a Shimadzu RI detector 20-A. The mobile phase was THF with a flow of 1 mL min^{-1} at 35 °C. Polystyrene (PS) standards were used for calibration and polymers characteristics obtained expressed according to those standards. Fourier-transform infrared spectroscopy (FTIR) was carried out with a Nicolet iS50 spectrophotometer (Thermo Scientific, USA), in transmission mode, in a range of 400–4000 cm^{-1} with a resolution of 2 cm^{-1} and 64 cumulative scans. Samples were compressed into KBr pellets (~1 mg of sample per 300 mg of KBr) before the analysis. X-ray diffraction (XRD) was performed with a Bruker D8-2 ADVANCE X-ray diffractometer for powders (Bruker, Germany), employing a Cu Kα X-ray source ($\lambda_{Cu\,K\alpha}$ = 1.54056 Å) and carrying out the analysis in a 2θ range of 10°–90°. A step size of 0.01° with a dwell time of 1 s per step was employed. Powders were placed on low-background PMMA sample holders prior to analysis. Bare, amino-functionalised and PDLLA-grafted BG samples were characterised by thermogravimetric analysis (TGA) using a TGA 2 Star System (Mettler Toledo). The analysis was performed

from 25 °C to 800 °C with a heating rate of 5 °C min^{-1} under N_2 atmosphere, then an isotherm of 10 minutes at 800 °C before the end of the analysis.

The ion release profile of the particles immersed in SBF was evaluated from the filtered SBF solutions collected at each time point by inductively coupled plasma optical emission spectroscopy (ICP-OES). Typically, solutions were diluted with demineralized water by a factor of 10, and analysed with an Agilent 5800 VDV ICP-OES in radial mode. The standard ranges were calibrated using single-element solutions. Diluted SBF was also analysed in order to obtain background values. The measurements were realised for all the sample solutions at each time point. Si, P, Ca and Cu concentrations were determined. The pH of every recovered sample solution was measured with a pHmeter inoLab pH7110 (3 points-calibrated with standards).

2.3.2. Evaluation of primary amine density, PDLLA grafting density and estimation of the molecular weight. The density of primary amines grafted on the surface of BG MPs samples was determined from TGA analysis by following the procedure described by Lagarrigue *et al.*[44] and illustrated extensively in the SI. To calculate the grafting density of the polymer, the second part of Lagarrigue's method could not be applied because the PDLLA calibration curve was realised with polymers having a specific molecular weight, which is not true for the grafting from approach. Thus, the PDLLA grafting density was roughly estimated by adapting the method used by Joubert *et al.*,[61] starting from the mass ratio between PDLLA and bare MPs with no organic species grafted. The mass of PDLLA is calculated from the TGA thermograms, and it is equal to the difference between the weight loss of PDLLA-BG and NH_2-BG above 150 °C (domains II + III). Then, the grafting density and molecular weight of the grafted chains were estimated by applying the method described in detail in the SI.

2.4. *In vitro* acellular evolution

Acellular *in vitro* tests for the bioactivity evaluation of the PDLLA-grafted BG samples were carried out by immersing the BG powders in SBF for up to 14 days (1, 3, 6, 24 hours, 7 and 14 days) at the physiological temperature (37 °C) and under constant agitation (200 rpm). All the conditions and experimental procedure applied for the bioactivity assessment were previously described.[60] The only difference was that the initial mass of polymer-grafted particles weighted for the tests was recalculated with respect to the percentage of polymer grafted in order to take exactly 100 mg of bare particles for each sample and respect the concentration of 3 mg mL^{-1}. The powders recovered from each time-point were characterised by SEM, FT-IR, XRD and EDX, while the SBF solutions recovered and filtered were analysed by ICP (in duplicate) and pH measurements (in triplicate). The samples were labelled as PDLLA-BG*x*-*y*, where *x* is the nominal amount of Cu and *y* is the specific time point (0 d, 1 h, 3 h, 6 h, 24 h, 7 d, 14 d).

2.5. Biological assessment

2.5.1. Antibacterial activity against *Escherichia coli*. Indirect antibacterial activity of particles was assessed by using the recovered and filtered SBF solutions of the *in vitro* acellular tests. Solutions at 1 hour and 14 days of BG and PDLLA-grafted BG immersion in SBF were selected for the evaluation, in order to compare the effect of the Cu^{2+} amount released in the medium. *Escherichia coli* (MG1655 strain) was cultivated in M9 medium (Na_2HPO_4 42.25 mM, KH_2PO_4 22.06 mM, NaCl 8.55 mM, NH_4Cl 18.7 mM, $MgSO_4$ 1 mM, glucose 5.84 mM, vitamin B1 3 mM) for 16 hours at 37 °C at 180 rpm. This bacterial culture was diluted 500 fold into fresh M9 medium in order to obtain exponentially growing culture. When $OD_{600\,nm}$ reached 0.04, cultures were diluted again 5 fold and exposed to the SBF solutions, at a ratio of 9.5 volumes of cultures for 0.5 volume of SBF. 200 μL of this mix was put into a well of a 96-wells plate, incubated at 37 °C with agitation (150 rpm) for 24 hours in Varioscan (ThermoFischer). The OD at 600 nm taken each 10 minutes were used to draw growth curves and to extrapolate from exponential phase the growth rate in h^{-1}. This growth rate was determined for each condition and each biological replicate. At the end of the 24 hours incubation, a sample was serially diluted and spotted (2.5 μL) on M9 agar plate and incubated overnight at 37 °C to evaluate the survival of the bacterial cells.

2.5.1. Fibroblasts L929 and preosteoblasts MC3T3-E1 cellular viability. Particles were exposed to UV-C (254 nm) for 5 minutes before addition of growth medium. Fibroblasts L929 were purchased from ECACC (NCTC-Clone 929, 85011425). The cells were maintained in DMEM high glucose (Sigma-Aldrich, D6546) supplemented with foetal bovine serum (5% v/v) (Gibco, 10270-106), 2 mM L-Glutamine (Gibco, 35050-038) and 100 U per mL of penicillin and 100 μg mL^{-1} streptomycin (Sigma-Aldrich, P0781) at 37 °C in a humidified incubator containing 5% CO_2. L929 cells were tested to be free of mycoplasma. The osteoblastic cell line MC3T3-E1 was purchased from ECACC (99072810). The cells were maintained in αMEM supplemented with 10% v/v foetal bovine serum (FBS), 2 mM L-Glutamine and 100 U per mL of penicillin and 100 μg mL^{-1} streptomycin at 37 °C in a humidified incubator containing 5% CO_2. MC3T3-E1 were tested to be free of mycoplasma. L929 and MC3T3-E1 were seeded at 1.0×10^4 cells per well in a 96-well plate and allowed to attach overnight under appropriate atmosphere. Thereafter, the medium was removed and replaced by 200 μL of the different suspensions of BG and PDLLA-grafted BG, prepared at 0.15 mg mL^{-1}, in the growth medium as well as the vehicle control. All dose groups were tested in at least 5 replicates. After 24 h and 48 h treatment, cell viability was assessed by MTS assay (abcam, ab197010) and Brightfield microscopy. Live&Dead (Invitrogen, L3224) staining was done after 24 h and 48 h as well. Positive cell culture controls were realised and called TCPS (tissue culture polystyrene).

2.6. Statistical analysis

The molar composition determined by SEM-EDX was estimated over a 100 μm^2 square of the sample through the P/B ZAF method, and the values were averaged over four measurements. Considering SBF tests, a triplicate powder suspension sample

was prepared for each time point and for each PDLLA-BG synthesised, for SBF tests. The powders of the triplicate sample for each time point were finally joined together, in order to have enough amount of each sample to be characterised. The ICP-OES analysis were realised for all the sample solutions at each time point in duplicate. Si, P, Ca and Cu concentrations were determined and the data points were presented as averaged values ± standard deviation for $n = 2$. The pH was measured in triplicate and results presented as averaged values ± standard deviation for $n = 3$.

3. Results and discussion

3.1. Synthesis and characteristics of PDLLA grafting

Four kinds of core–shell bioactive glass microparticles/PDLLA were synthesised with a three steps procedure: (i) synthesis of spray-dried bioactive glass microspheres with varying amounts of Cu doping, already described in our previous work[60]; (ii) amino-functionalisation of the bare BG samples (Fig. 1a); (iii) surface-initiated ROP of D,L-lactide from the surface of amino-functionalised BG MPs (Fig. 1b and Table 1). A further step was to separate the free residual PDLLA chains. After separation, the free PDLLA and the PDLLA-grafted BG microspheres were characterised respectively by SEC (to determine molecular weight and dispersity ($Đ$)) and by SEM, FTIR, and TGA (to assess the density of primary amines and the amount of PDLLA on the microsphere surface).[44,61]

As the micrographs of the four PDLLA-grafted samples are very similar to each other, and likewise for the four non-grafted samples, only the images of the 0-BG bare and grafted particles are shown in Fig. 2 (the complete set of micrographs is available in Fig. S3). Compared to non-functionalized particles, the grafted MPs show a greater tendency to agglomerate in the dry state, which may be partially caused by the drying conditions. However, the primary objective of the present work is not to prevent dry-state agglomeration, but rather to avoid the aggregation and rapid sedimentation of bare, hydrophilic bioactive glass particles in apolar organic solvents (such as dimethyl carbonate) used for freeze-casting processes, where PDLLA grafting significantly improves colloidal stability and dispersion. Additionally, the observed aggregates appear to be enveloped in a layer with a texture distinct from that of bare BG samples. This layer, visible in the interstitial spaces between individual particles, blurs their contours and is likely attributable to the polymer corona formed on the MPs surface.

Before conducting a more detailed characterisation of the PDLLA grafted onto the particles, attention can be given to the free PDLLA chains separated from the grafted ones and analysed by SEC which, by analogy, can provide insight into the behaviour of their grafted counterparts. The four traces were shown in Fig. S4, whereas molecular weights and dispersity values were reported in Table S4. The results indicate much higher molecular weights than expected for the grafted chains, probably due to the uncontrolled polymerisation initiated by moisture or impurities in solution, except for the samples PDLLA-BG0 (M_n = 21 000 g mol^{-1}) and PDLLA-BG5 (M_n = 32 000 g mol^{-1}). The high dispersity values obtained for ROP in solution (1.5–2.2) are in line with a partially controlled polymerisation, which is typically attributed to the presence of residual moisture

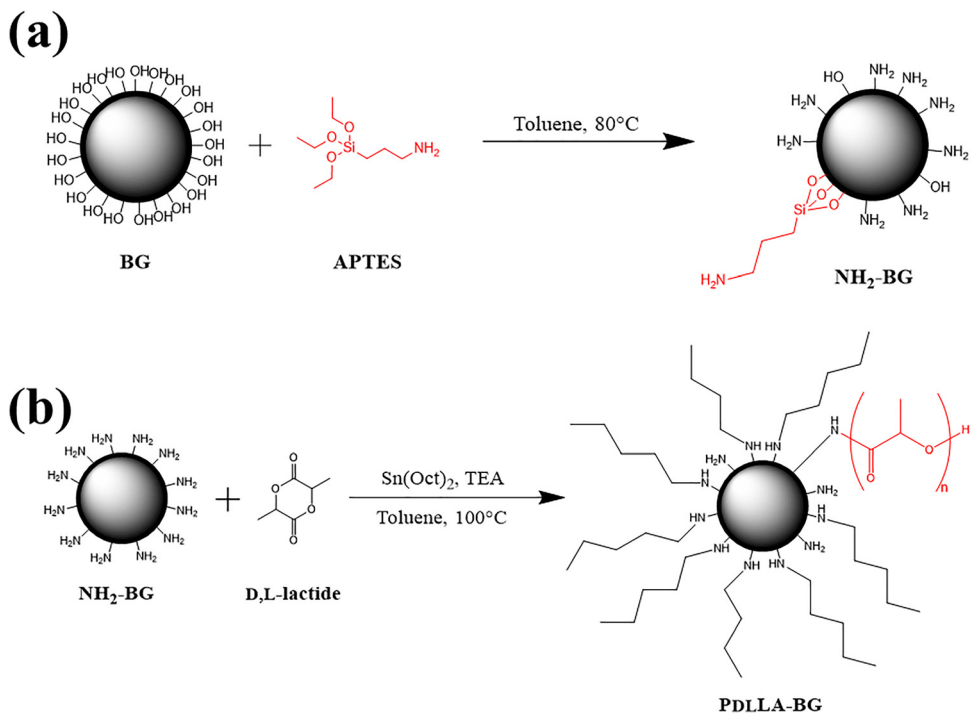

Fig. 1 Synthetic pathway illustrating (a) the amino-functionalisation of bioactive glass microparticles with (3-aminopropyl)triethoxysilane (APTES) and (b) the surface-initiated ring-opening polymerisation (ROP) of D,L-lactide from the amino-functionalised microparticle surface.

Table 1 Synthesis parameters for the surface-initiated ROP of D,L-lactide from the surface of amino-functionalised spray-dried quaternary bioactive glass microparticles and corresponding DP and Mn

Sample	n_{APTES} (mmol)	ρ_{NH_2} ($mmol_{NH_2}$ g_{MPs}^{-1})[a]	[In]/[Mon]/[TEA]/[Sn] (eq.)	Conv. (%)[b]	$M'_{n,th}$ (g mol^{-1})[c]	σ_{PDLLA} (#chains nm^{-2})[d]	σ_{PDLLA} (μmol g_{MPs}^{-1})[e]	n_{PDLLA} (mmol)[f]	$M_{n,exp}$ (g mol^{-1})[g]
PDLLA-BG0	16.3	0.167	1/167/0.5/0.2	94	22 600	0.34	2.09	0.209	21 600
PDLLA-BG1	15.3	0.156	1/177/0.5/0.2	97	24 700	0.38	2.01	0.201	23 600
PDLLA-BG2.5	15.5	0.158	1/175/0.5/0.2	96	24 200	0.60	3.44	0.344	22 300
PDLLA-BG5	12.7	0.129	1/215/0.5/0.2	95	29 400	0.24	1.48	0.148	28 200

[a] Determined from eqn (S5). [b] Determined from eqn (S8). [c] Determined by multiplying $M'_{n,th}$ by the monomer conversion. [d] Determined from eqn (S9). [e] Determined from eqn (S10). [f] $n_{PDLLA} = 100\ \sigma_{PDLLA}$ (μmol g^{-1}). [g] Determined from eqn (S11).

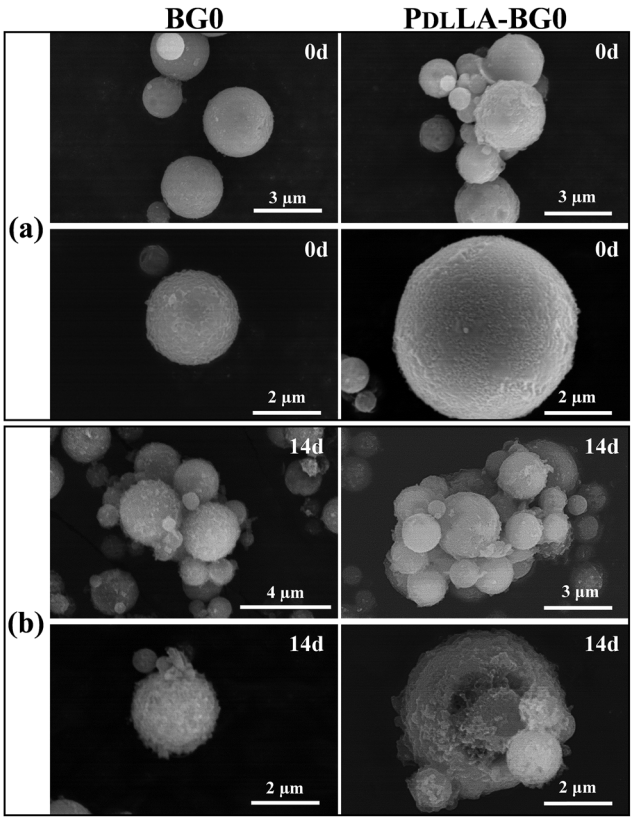

Fig. 2 SEM micrographs of (a) as-synthesised bare BG0 and PDLLA-BG0 particles, shown as agglomerates (top) and individual particles (bottom), and (b) the same samples after 14 days of immersion in SBF.

or impurities, as frequently encountered when using tin(II) octanoate as catalyst.

PDLLA-grafted BG samples were characterised by FT-IR analysis in order to confirm the successful grafting of PDLLA onto the particles surface. The spectra exhibit almost the same behaviour. Therefore, only the spectra of the bare and grafted BG0 particles are presented in Fig. 3a–c, while the full set of spectra is provided in Fig. S5a, b and Fig. S6a–c, for bare and polymer-grafted samples, respectively.

The vibrations of the silica network typical of bioactive glasses are identified at 1100 cm^{-1}, 815 cm^{-1}, 466 cm^{-1}, corresponding to the asymmetric stretching, bending, and rocking vibrations of the siloxane bond (Si–O–Si), respectively.[56–58] At 604 cm^{-1} and 564 cm^{-1} two small bands can be observed, standing for the bending and stretching vibrations of PO_4^{3-} ions in a CaP environment, both apatitic and non-apatitic.[59–61,64–66] Regarding the PDLLA presence for grafted particles, the small bands at 3000 cm^{-1}, 2950 cm^{-1} and 2925 cm^{-1} were assigned to the symmetric and asymmetric stretching of the C–H bond of the PDLLA methyl group, and to the stretching of the C–H bond belonging to the APTES ethylene groups.[22,53] The strongest band detected for the PDLLA backbone is found at 1767 cm^{-1}, typical of the C=O stretching of the ester group, while other small bands are identified at 1456 cm^{-1} ($-CH_3$ bending), 1387 cm^{-1} (C–H symmetric bending deformation) and 930 cm^{-1} (C–C stretching).[22] A small band at 1541 cm^{-1}, and a weak and broad band around 700 cm^{-1}, were identified respectively to the N–H in-plane and out-of-plane bending vibrations of the secondary amide bond,[68] thus providing spectroscopic evidence consistent with the successful grafting of PDLLA chains onto the MPs surface. Another evidence of the successful amidation might be found in the broadened band belonging to the physiosorbed water in the range 1600–1700 cm^{-1}, which might overlap with the vibration of the C=O stretching of the amido bond at 1641 cm^{-1}.[68] Finally, the broad band at 3430 cm^{-1} may be attributed to the contribution of either free and hydrogen bonded silanol groups with water (Si–OH and Si–OH$\cdots H_2O$ stretching vibration[63]), but also to the N–H stretching band.

3.2. Grafting density by thermogravimetric analysis

Thermogravimetric analysis was performed on bare, amino-functionalised and PDLLA-grafted MPs with the purpose to evaluate the grafting density of APTES molecules and PDLLA chains on MPs surface, as well as to estimate the molecular weight of the grafted polyester. The thermograms of BG0 NH_2-BG0 and PDLLA-BG0 were shown in Fig. 3d, while the full set of thermograms is illustrated in Fig. S6d–g, and they were all divided into three zones, according to the thermal degradation of the chemical species:

•Domain I (25–150 °C): evaporation of the physiosorbed water on the MPs surface;

•Domain II (150–350 °C): thermal degradation of grafted PDLLA chains, overlapped to the condensation of superficial silanol groups[46,69,70];

•Domain III (350–800 °C): thermal degradation of aminopropyl groups from grafted APTES molecules, overlapped to the condensation of internal silanol groups.[70,71]

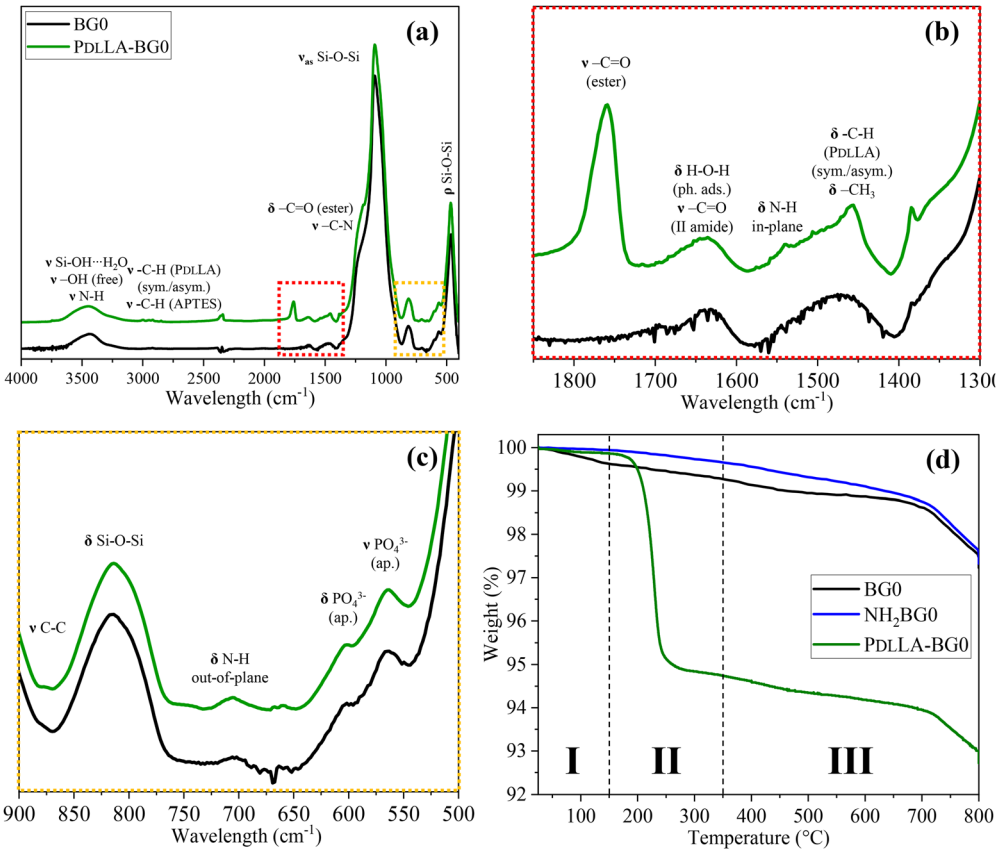

Fig. 3 (a) Stacked FT-IR spectra (in absorbance) of BG0 and PDLLA-BG0, with enlarged views of the (b) 1300–1800 cm^{-1} and (c) 500–950 cm^{-1} regions. (d) TGA thermograms of BG0, NH_2-BG0, and PDLLA-BG0.

The weight loss percentages (Δm) for all analysed samples in each domain are summarised in Table S5. The density of grafted amines was characterised using the same methodology described by Lagarrigue *et al.*[44] and the corresponding values are presented in Table 1 and Table S2. The grafting density (ρ_{NH_2}), expressed as the number of APTES molecules per nm^2 of MP surface, ranges between 20 and 30 $\#NH_2$ nm^{-2}, significantly higher than the values reported for NH_2-BG NPs in Lagarrigue's study. However, the molar amount of primary amines per gram of NH_2-BG particles is lower. This apparent paradox arises from the lower surface area of MPs compared with NPs: fewer accessible sites per gram of microparticles result in a lower total number of grafted molecules, despite a higher surface functionalisation density. Importantly, the same initial amount of APTES per gram of particles was applied to all samples, regardless of their specific surface area.

The conversion of lactide monomer for the synthesis of grafted BG MPs was almost quantitative (94–97%). The theoretical molecular weights calculated by considering the monomer conversion are between 22 000 and 30 000 $g{\cdot}mol^{-1}$ (Table 1). The grafting densities of PDLLA chains were estimated using TGA and eqn (S9) and (S10). These grafting densities ranged from 0.24 to 0.60 chains per nm^2 of MPs surface, with the σ_{PDLLA} of PDLLA-BG2.5 being the highest value.

These values are higher than those reported previously,[44] owing to the specific surface area differences mentioned above. Consequently, the amount of polyester grafted per gram of MPs is considerably lower. In addition, the experimental molar masses were estimated using eqn (S11). The measured molecular weights are in good agreement with the theoretical values, confirming successful grafting and the presence of long polymer chains in the 22 000–28 000 g mol^{-1} range. All these results are summarised Table 1. No significant differences in grafting efficiency were observed among the samples, indicating that the surfaces of the four spray-dried bioactive glass microparticles are essentially identical, irrespective of their Cu content.

To conclude this section, we demonstrated the successful synthesis of core–shell bioactive glass/PDLLA particles using a "grafting from" strategy. The resulting grafting density of PDLLA chains was higher than that typically achieved with a "grafting to" approach (0.2 chains·nm^{-2}).[44,45] Although surface-initiated polymerisations can be affected by competitive chain-growth mechanisms, leading to increased dispersity ($Đ$) of the grafted polymers and reduced control over their final properties, "grafting from" offers a clear advantage by reducing the number of experimental steps. In this case, ring-opening polymerisation (ROP) occurs directly from the particle surface, with surface amination being the only required functionalisation. Moreover, this approach appears to allow the achievement of high molecular weights, which is difficult to obtain with

"grafting to" methods because of steric hindrance and limited accessibility of the particle surface.

3.3. Acellular *in vitro* evolution of PDLLA-grafted BG MPs in SBF solution

The *in vitro* acellular behaviour of the grafted particles in SBF was evaluated and compared with that of bare particles to assess the influence of the polymer-grafted corona on the morphological, physicochemical, and ion-release changes of the bioactive glasses, with particular attention to copper release kinetics. As a reminder, our previous study[60] showed that the bare particles generated by spray-drying were mainly composed of a silicate glassy network, in which, depending on the copper concentration, phosphate and calcium ions were incorporated into the network (as co-former and network modifiers, respectively), while copper atoms were integrated either as Cu^{2+} network modifiers and Cu^0 nanoparticles. In the same work, the distribution between copper ions and metallic copper was accurately investigated by combining electron paramagnetic resonance (EPR) and quantitative EDX using a calibrated standard, and the Cu^{2+}/Cu^0 ratios were reported for as-synthesized samples and after immersion in SBF.

The PDLLA-grafted BG samples were characterised at each time-point by FT-IR and XRD analysis. FT-IR spectra showing the evolution of bare and PDLLA-BG samples before soaking in SBF and after 14 days immersion are presented in Fig. 4a, while the full set of spectra of all the time points representing the evolution of PDLLA-BG0, PDLLA-BG1, PDLLA-BG2.5 and PDLLA-BG5 in SBF are provided in Fig. S8a, c, e and g, respectively. For comparison, FT-IR spectra from the degradation study on bare BG samples are reported in Fig. S7a, c, e and g for BG0, BG1, BG2.5 and BG5, respectively. The spectra of all the polyester-grafted samples at each time-point display an evolution similar to that of bare samples. For instance, the gradual increase of the orthophosphate band (500–650 cm^{-1}) with the soaking time, along with the emergence of two distinct bands at 604 cm^{-1} and 564 cm^{-1} (PO_4^{3-} stretching in apatitic environment) starting from 24 h onwards, constitute a qualitative indication of nanocrystalline apatite formation. In this case, no significant difference in the PO_4^{3-} band was observed as a function of the copper content. Furthermore, the vibration of carbonate group (CO_3^{3-} stretching) is detected at 880 cm^{-1}, indicates the presence of a small amount of carbonated nano-hydroxyapatite (nHCA).[72] Therefore, the main distinction between PDLLA-grafted and bare samples is that the former had additional bands belonging to the polyester chain backbone, with the most intense band located at 1767 cm^{-1} (C═O stretching of the ester groups). Notably, the intensity of this band progressively decreases with the immersion time in SBF. In some cases (*e.g.*, PDLLA-BG0-14d and PDLLA-BG5-14d), this band is barely detectable. Thus, the reduction in carbonyl band intensity can be regarded as a qualitative marker of PDLLA degradation in the medium, associated with random chain scission by hydrolysis.

XRD diffractograms representing the evolution of bare and PDLLA-BG samples before soaking in SBF and after 14 days immersion are presented in Fig. 4b, while the complete set of diffractograms of all the time points representing the evolution of PDLLA-BG0, PDLLA-BG1, PDLLA-BG2.5 and PDLLA-BG5 in SBF are provided in Fig. S8a, c, e and g, respectively. For comparison, XRD diffractograms of the degradation study on bare BG samples were reported in Fig. S7a, c, e and g for BG0, BG1, BG2.5 and BG5, respectively.

As confirmed by FT-IR analysis, XRD diffractograms follow the same overall trend as those of bare BG samples. Similarly, the peaks associated with Cu^0 nanoparticles remain unchanged, while the broad diffraction peak of nanocrystalline hydroxyapatite (211) at 31.8° gradually increases, becoming more evident after 24 h. As reported in previous work, the main sharp peak of calcite ($CaCO_3$) appears at 29.4°, although only in some diffractograms and with variable intensity. The occurrence of calcite, as already discussed, is most likely due to random homogeneous nucleation induced by the high concentration of Ca^{2+} and carbonate ions in solution. The main difference compared with as-synthesised BG diffractograms is the appearance of a new peak at 18°, observed only in Cu-doped PDLLA-BG samples after 7 and 14 days of immersion in SBF. This relatively sharp diffraction peak can be attributed to the main diffraction

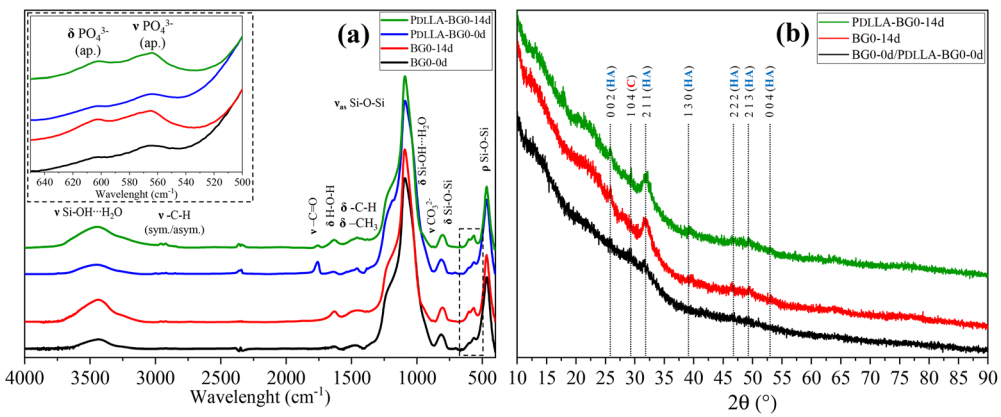

Fig. 4 (a) FT-IR spectra (in absorbance) of BG0 and PDLLA-BG0 particles with enlarged 500-650 cm^{-1} region, prior to soaking in SBF and after 14 days degradation; (b) XRD diffractograms of BG0 and PDLLA-BG0 particles, prior to soaking in SBF and after 14 days degradation.

plane of copper hydroxyphosphate ($Cu_2(OH)PO_4$) (JCPDS card File No. 36-0404).[73,74] This phenomenon may be explained by local acidification of the medium, in phosphate- and copper ion-rich regions, as a consequence of PDLLA degradation.

SEM micrographs of bare and grafted BG0 after 14 days of degradation are presented in Fig. 2b, while additional images after 24 h, 7 days, and 14 days of immersion in SBF are reported for bare and PDLLA-grafted samples in Fig. S9 and S10, respectively. From the first day of immersion, both grafted and bare particles are mainly observed as large agglomerates, similar to their state prior to soaking, although significant morphological modifications occur upon degradation. After 24 h, a newly formed layer becomes visible, particularly in the interstices between particle aggregates. Based on its characteristic rough "cauliflower-like" morphology, this layer can be attributed to hydroxyapatite, clearly distinguishable from the smoother and more homogeneous polymer coating initially covering the large MP aggregates. However, this mineral phase develops in a heterogeneous manner. Its growth appears more pronounced in samples with lower PDLLA content, likely due to polymer degradation that locally exposes the surface to ionic exchange, as evidenced in micrographs of PDLLA-BG0-24h and PDLLA-BG5-24h. After 7 days, both individual particles and their aggregates are covered by a homogeneous mineral layer, closely resembling the morphology observed for bare BG samples at the same time point. At this stage, particle boundaries are no longer discernible, as in PDLLA-BG0-7d. Interestingly, in the group image of PDLLA-BG2.5-7d, remnants of the polyester layer remain visible, with hydroxyapatite domains deposited preferentially in superficial regions where grafted PDLLA has presumably degraded. After 14 days of soaking, the samples display similar morphological features. However, it remains challenging to determine whether the amount of newly formed mineral phase has further increased compared to the 7-day stage.

EDX compositional analysis was carried out on polymer-grafted samples immersed for 14 days in SBF, and the at% values of the elements composing the PDLLA-BG samples with respect to the bare BG MPs prior to soaking (labelled "as-synthesised") were reported in Table 2. For comparison, the at% composition of bare BG samples after 14 days was reported as well.

From the EDX results, it is difficult to clearly assess how the absolute Si content decreases in both bare and PDLLA-grafted samples compared with pre-soaking values, since its relative proportion (with respect to other elements) appears higher in polymer-grafted particles (ranging from +2.6% to +7.7%, depending on the sample). Conversely, the phosphorus content increases significantly compared to both pre-immersion particles and bare BG samples after 14 days in SBF, while the relative calcium content markedly decreases. Interestingly, the Ca/P ratio (Table S6) decreases by about 50% compared to pre-immersion values, thus reversing the trend observed in bare BG samples, where Ca/P slightly increases after 14 days of evolution.[54] The Ca/P ratios measured for PDLLA-grafted samples are closer to the stoichiometric value of hydroxyapatite (particularly for Cu-doped samples), suggesting that nearly all Ca^{2+} and PO_4^{3-} ions are involved in the formation of nanocrystalline HA. These findings corroborate the presence of hydroxyapatite previously identified by FT-IR and XRD analysis. However, it remains uncertain whether apatite is the only phase formed after immersion, since XRD diffractograms revealed an additional peak at 18° in Cu-doped PDLLA samples at longer time points. The relatively high phosphorus content detected in polymer-grafted samples (especially those doped with Cu) may indicate that a slight excess of phosphate (possibly incorporated in the silica network and located near Cu^{2+} ions) contributes to the precipitation of copper hydroxyphosphate, triggered by local acidification of the medium during PDLLA degradation.[67,68] This hypothesis is further supported by the observation that phosphorus content increases substantially, while copper levels do not decrease accordingly, suggesting that the higher local availability of PO_4^{3-} and Cu^{2+} ions favours the formation of copper hydroxyphosphate microcrystals. Considering the Cu presence, any substantial change was detected.

3.4. Ion release profile

The ion release profiles of PDLLA-grafted BG samples were determined by ICP-OES for Si, P, Ca, and Cu, by analysing SBF solutions collected from 1 h to 14 days of immersion (in duplicate, including the initial SBF solution). The copper release results are shown in Fig. 5, while those for Si, P, and Ca are reported in Fig. S12, with an inset focusing on the earliest time points (0 d, 1 h, 3 h, 6 h). For comparison, ion release data from bare BG samples are presented in Fig. S11. Overall, all samples display similar release trends for each element, although with some differences in concentration values.

Table 2 EDX analysis of compositional changes in bare and PDLLA-grafted BG samples after 14 days of immersion in SBF (14 d), compared with the initial microparticles (as-synthesised)

					Elemental composition (at%) determined by EDX											
	Nominal composition (at%)[a]				As-synthesised[a]				BG 14d				PDLLA-BG 14d			
Sample	Si	P	Ca	Cu	Si	P	Ca	Cu	Si	P	Ca	Cu	Si	P	Ca	Cu
#1	67.5	7.5	25.0	0.0	63.1	6.0	30.9	0.0	59.0	6.0	35.0	0.0	69.5	8.1	22.3	0.0
#2	67.5	7.5	24.0	1.0	65.6	6.6	26.7	1.1	62.1	7.0	30.1	0.8	70.7	9.6	18.6	1.0
#3	67.5	7.5	22.5	2.5	62.7	7.3	26.9	3.2	62.9	7.3	27.7	2.1	70.4	9.9	16.9	2.9
#4	67.5	7.5	20.0	5.0	66.5	7.0	20.9	5.6	61.5	8.0	26.0	4.5	69.1	10.5	14.8	5.6

[a] Values corresponding to the composition of both bare BG and PDLLA-grafted samples, as-synthesised (prior to immersion in SBF).

As expected, the ion release profiles generally follow the same behaviour as bare samples, indicating that the proposed degradation mechanisms, structural modifications, and release kinetics also apply to polymer-grafted samples. However, a systematic decrease in ionic concentrations is observed.

For example, the Si release (Fig. S12a) in the first hours of immersion reaches ~60 ppm depending on the sample, which is 10–30 ppm lower than the corresponding values for bare BG. The *P* concentration profile (Fig. S12c) follows the same trend as bare samples, showing slightly higher values in the first hours, but becoming undetectable after 24 h. Regarding Ca^{2+} evolution (Fig. S12e), the drastic reduction reported at 24 h in the previous study is still observed, but it appears considerably attenuated: PDLLA-BG0, PDLLA-BG1, and PDLLA-BG2.5 suspensions lose only ~15 ppm of Ca^{2+} between 6 h and 24 h, while in PDLLA-BG5, the calcium concentration remains unchanged. Moreover, the amount of Ca^{2+} released in the first hour is significantly lower than in bare BG samples, ranging between 175 and 250 ppm depending on the formulation. The Cu^{2+} release profile (Fig. 5) shows the same trend: a reduced ion release in the first few hours, but reaching, after 14 days, the same concentrations observed for the bare samples.

As observed in all ion release profiles, the amount of species leached during the first few hours is generally lower compared to bare BG particles. This highlights a marked reduction of the so-called burst effect, *i.e.* the rapid ion release occurring immediately after BG powders are immersed in solution. This phenomenon is typically caused by the substitution of H^+, H_3O^+, and H_2O for network modifiers (Ca^{2+} and Cu^{2+}), followed by hydrolytic dissolution of the silica network. Accordingly, the ionic concentrations measured at the earliest time points in polymer-grafted samples are consistently lower than those of bare BG.

For the same reason, the phosphorus release profile decreases with a slightly reduced slope, although phosphate ions are no longer detectable after 24 h. This behaviour can be explained by the presence of a PDLLA corona surrounding the MPs. Thanks to its hydrophobic character, the polymer coating shields the particle surface, limiting the glass area in direct contact with the medium and thereby reducing the extent of ionic exchange. This shielding effect is consistent with the pH evolution shown in Fig. S12b: since pH variations indirectly reflect the degree of ionic exchange, the lower shift observed for grafted samples (compared with bare BG, Fig. S12a) confirms a reduced silica network dissolution rate, and consequently a lower release of other ionic species. Moreover, the slight pH decrease is likely due to a buffering effect caused by PDLLA hydrolysis, which generates additional H^+ in the medium. However, this "shielding" effect appears to be effective only during the first hours of soaking. Once the polyester chains start to degrade (as indicated by the reduction of the C=O FT-IR band), the bioactive glass surface becomes increasingly exposed to SBF, and ionic exchange rises again. Although this subsequent mineralisation step is not directly evident from the ion release profiles, it is confirmed by SEM observations, FT-IR spectra, and XRD diffractograms, all showing hydroxyapatite formation after 24 h for most samples. As in our previous study,[54] nanocrystalline apatite formation on the BG surface proceeds through two mechanisms: (i) recombination of PO_4^{3-} with Ca^{2+} in solution, followed by precipitation of nHA, and (ii) gradual conversion of ACP nanodomains (initially present in the particles) into nanocrystalline apatite through water uptake and crystallisation. The main difference here is that the first mechanism is likely reduced and/or delayed due to the lower calcium release during the early stages. In addition, the slightly lower pH is less favourable to hydroxide species such as HA. An additional noteworthy point concerns the ion release profile of PDLLA-BG5 during the initial hours of immersion. The extent of ionic exchange is lower than in the other three samples, and copper release kinetics at 1 h appear significantly slower than for PDLLA-BG2.5. After this period, however, the Cu^{2+} concentration rises more rapidly. This effect may be related to the molecular weight of the grafted polymer, which is the highest for PDLLA-BG5 (M_n 28 200 g mol^{-1}), suggesting that polymer chain length plays a more decisive role than grafting density in governing (and here enhancing) the shielding effect.

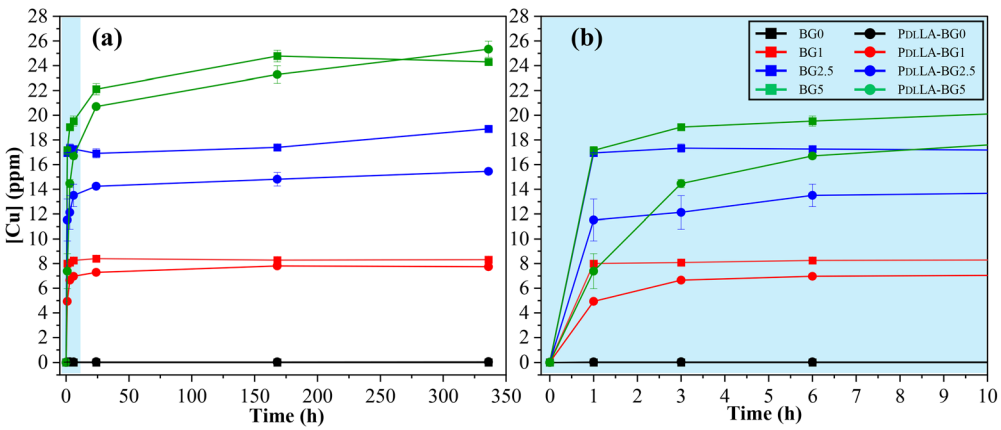

Fig. 5 (a) Copper ion release profiles of bare spray-dried BG and PDLLA-grafted BG samples during *in vitro* acellular tests in SBF, monitored from 0 to 14 days. (b) Enlarged view of the early time points (0 d, 1 h, 3 h, 6 h). Each data point represents the Cu concentration measured in SBF at the corresponding time.

Concerning the doping-dependent behavior of copper release, the Cu^{2+}/Cu^0 ratio in the initial formulation of the microspheres also represents a fundamental parameter, since a higher Cu^{2+} content results in an enhanced burst effect, as previously demonstrated.[54] However, the fraction of copper present as Cu^0 clusters acts as a reservoir for long-term release. Even at medium time scales, and despite the slower release kinetics observed for the PDLLA-grafted particles, the total amounts of copper delivered differ: 16.9–24.6% and 21.0–30.8% of the initially incorporated copper are released for BG and PDLLA-BG samples, respectively. Indeed, the possible degradation of Cu^0 nanoparticles should also be considered, as these may be particularly sensitive to the local increase in H^+ concentration induced by PDLLA hydrolysis.

3.4. Biological assessment

The antibacterial activity against *E. coli* was evaluated through indirect assays using the SBF solutions, whereas cell viability was assessed by culturing murine fibroblasts and preosteoblasts in direct contact with the particles. The objective was to investigate the correlation between the polymer corona, Cu^{2+} release, and the biological responses, in order to determine whether the presence of the PDLLA shell provides a beneficial effect for the intended application.

3.4.1. Antibacterial potential against *E. coli*. The antibacterial activity of BG and PDLLA-grafted BG particles was indirectly assessed using the recovered and filtered SBF solutions (sample C of the triplicates) obtained from *in vitro* acellular tests. Solutions collected after 1 h and 14 days of immersion were selected to evaluate in particular the impact of Cu^{2+} release on bacterial growth. The 1 h SBF solutions reflect the initial burst of copper released by bare and PDLLA-grafted BG samples, while the 14-day solutions represent the maximum Cu^{2+} concentration reached during the acellular experiments. As previously discussed, the study also aimed to determine how polymer grafting influences bacterial growth inhibition. Indeed, PDLLA-grafted BG samples exhibited a markedly reduced burst release of copper in SBF compared to bare BG MPs, although the concentrations measured at 14 days were comparable or slightly lower. For antibacterial activity testing, *E. coli* (MG1655 strain) was chosen owing to its predictable behaviour and ease of handling. *E. coli* cultivated in M9 medium was mixed with the SBF solutions and distributed into 96-well plates. The optical density ($OD_{600\,nm}$) was recorded over 24 h to obtain bacterial growth curves and calculate growth rates. After incubation, aliquots of each bacterial culture/SBF mixture were plated on agar to evaluate the survival of *E. coli* cells.

The growth rates of *E. coli* cultures, determined from OD_{600} measurements after 24 h incubation with SBF solutions, are graphically illustrated in Fig. 6. For non-functionalised BG MPs (Fig. 6a), the observed growth rates are consistent with the Cu release profiles measured by ICP. Specifically, exposure to BG2.5 and BG5 SBF solutions (collected after either 1 h or 14 days of immersion) significantly reduced bacterial growth rates by 40–44% and 70–85%, respectively, compared to BG0. No significant difference was observed between the 1 h and 14 d solutions, confirming the ICP results and the rapid Cu^{2+} burst release upon immersion. The only exception was BG5, where the growth rate further decreased between 1 h and 14 d, consistent with the progressive increase in Cu^{2+} release over time. Then, in general, the bare BG samples inhibited bacterial growth in a Cu dose-dependent manner. In contrast, SBF solutions from PDLLA-grafted BG samples (Fig. 6b) showed a different trend. After 1 h of immersion, the growth rate was $\sim$1.2 h^{-1} for all tested samples, indicating no detectable influence of Cu content at this stage. Moreover, these values were slightly higher than those from bare BG samples, reflecting the reduced Cu release from PDLLA-grafted particles (shielding effect). At 14 days, however, the SBF solutions displayed a more pronounced antibacterial effect, with PDLLA-BG5 completely inhibiting *E. coli* proliferation.

These results are consistent with the macroscopic views from the survival tests shown in Fig. S14 at different serial dilutions, where the same trends observed in the previous analyses can be visually confirmed for both bare and PDLLA-grafted BG samples. Overall, the data indicate that Cu^{2+} ions released in SBF inhibit *E. coli* growth in a dose-dependent manner but do not completely eradicate the cells, with the

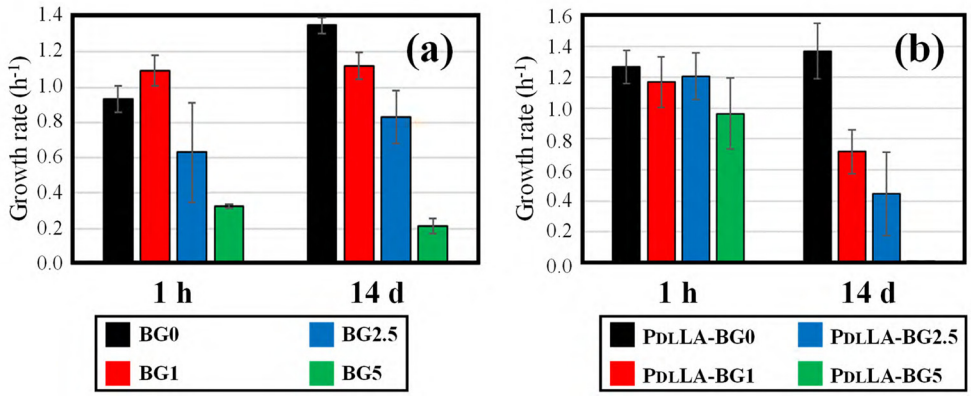

Fig. 6 Bar chart representation of *E. coli* growth rates (along with their standard deviations) in contact with SBF solutions collected after 1 hour and 14 days of BGx (a) and PDLLA-grafted BGx immersion (b).

exception of PDLLA-BG5, which totally stops the bacterial growth. The delaying effect of the polyester corona is also evident in SBF solutions after 1 h of soaking. The limited Cu^{2+} release observed over 14 days (relative to the total copper content) suggests that Cu^0 nanoparticles embedded within the BG matrix may degrade only after complete breakdown of the glass network, thereby sustaining copper ion release over extended periods.[75,76]

The antibacterial activity can thus be modulated by controlling both the amount and the release kinetics of copper. This study, combined with previous work,[60] demonstrates that at the scale of these particles, two levers can be activated to achieve a prolonged and effective release: (i) the formulation of the bioactive glass (for example, by using more reactive phosphate precursors to enhance the incorporation of Cu^{2+}[71]). In practice, tuning the Cu^{2+}/Cu^0 ratio provides a way to balance the antibacterial response: increasing Cu^{2+} incorporation into the silicate network (at the expense of Cu^0 nanoparticles) would intensify the initial copper release but shorten its duration, whereas a higher proportion of Cu^0 would prolong the antibacterial effect over time. (ii) the presence of PDLLA chains, whose primary role is to provide mechanical cohesion to the scaffolds resulting from the assembly of the microparticles/'bricks' studied in this work. Their hydrophobic character, together with the acidity arising from their hydrolytic degradation, may directly or indirectly (through their influence on bioactive glass degradation) affect the antibacterial behaviour.

3.4.2. Cytotoxicity assessment. The cytotoxicity of bare and PDLLA-grafted BG samples was assessed by direct contact with cells cultured in a 96-well plate. Two distinct cell lines were employed: fibroblasts (L929) and pre-osteoblastic cells (MC3T3-E1). After 24 and 48 h of incubation, cell viability was evaluated using the MTS assay. In addition, cells incubated for 24 and 48 h were examined by Brightfield and fluorescence microscopy following live/dead staining. The viability results for fibroblasts and pre-osteoblasts, obtained from MTS assays after treatment with the MP suspensions, are presented in Fig. 7a and b, respectively.

The MTS assay is a colorimetric method for the sensitive quantification of viable cells. It relies on the reduction of the MTS tetrazolium compound by metabolically active mammalian cells to form a soluble formazan dye in the culture medium. This reaction is believed to be catalysed by NAD(P)H-dependent dehydrogenase enzymes. The amount of formazan formed is quantified by measuring the absorbance at 490 nm, where higher absorbance values correspond to higher metabolic activity of the tested cells. An increase in cell viability between 24 h and 48 h, observed in most samples, indicates active cell proliferation. The relatively high standard deviation calculated for both cell lines at 48 h arises from the fact that cell viability values represent the average of $n = 2$ tests out of a total of $n = 5$.

For the L929 fibroblast plot, neither the bare nor the polymer-grafted ternary samples exhibited significant cytotoxicity compared with the positive control. Bare samples showed a dose-dependent decrease in cell viability at both 24 h and 48 h, with higher Cu content leading to stronger effects: BG5

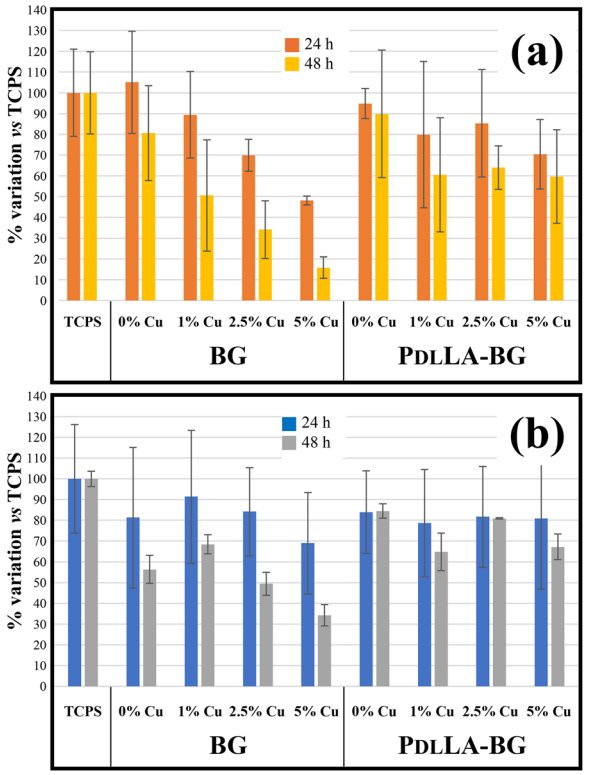

Fig. 7 Cell viability of (a) L929 fibroblasts and (b) MC3T3-E1 pre-osteoblastic cells after treatment with bare and PDLLA-grafted BG samples for 24 and 48 h in culture medium, expressed as percentage variation with respect to the positive cell culture controls (TCPS). For L929, MTS values represent the mean of $n = 4$ tests at 24 h and $n = 2$ tests at 48 h, whereas for MC3T3-E1 the plotted values correspond to the mean of $n = 2$ tests at both time points.

displayed the highest cytotoxicity. In contrast, PDLLA-grafted BG samples exhibited higher viability than bare samples at the same Cu doping level: all are cytocompatible except PDLLA-BG5, which showed slight cytotoxicity. These results indicate that the polymer corona positively influences fibroblast viability in direct contact with the particles. For the MC3T3-E1 pre-osteoblastic cell line, a similar dose-dependent effect was observed for bare samples, with BG2.5 and BG5 showing cytotoxicity after 48 h. By contrast, PDLLA-grafted BG samples displayed comparable viability at 24 h regardless of Cu content. Moreover, as also observed with L929 fibroblasts, cell viability at 48 h was considerably enhanced for all compositions tested. Thus, MC3T3-E1 cells exhibited reduced sensitivity when exposed to the core–shell particles.

After interaction of both cell lines with the microparticles powders, the cultures were examined by Brightfield and fluorescence microscopy, the latter following incubation with live/dead dyes. Brightfield images of L929 cells treated for 24 h with bare BG and PDLLA-grafted BG samples are shown in Fig. S15a–h, respectively. Images of L929 cells treated for 48 h and MC3T3-E1 cells at both 24 and 48 h are not shown, as they exhibited patterns and cytotoxic effects similar to those already displayed. In the provided images, dark spots correspond to aggregates of

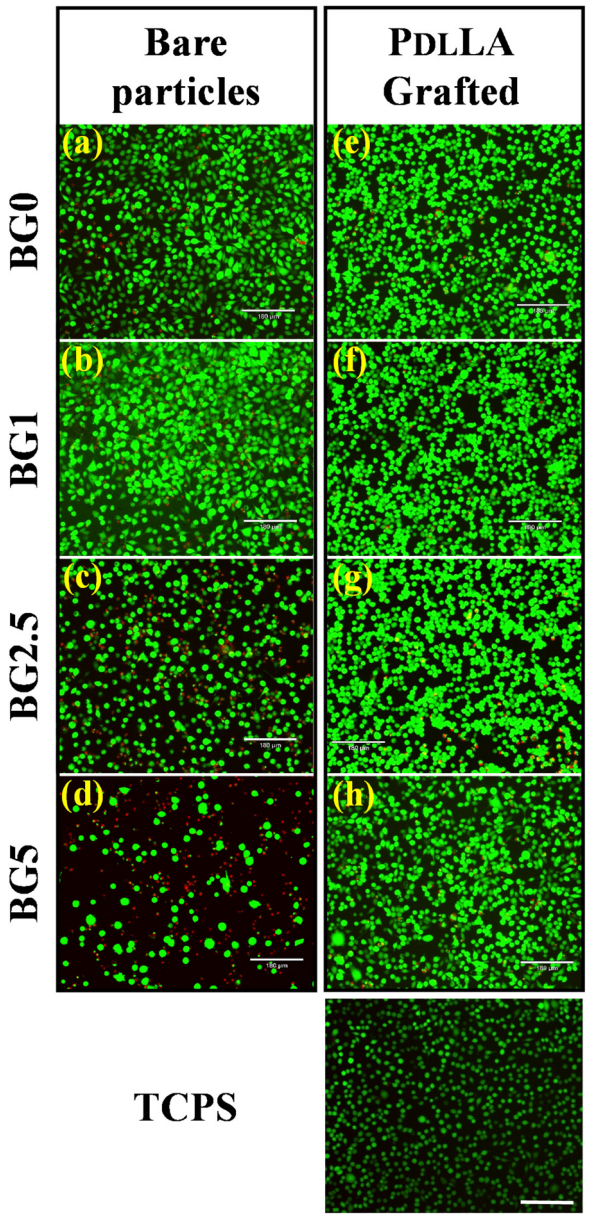

Fig. 8 Fluorescence microscopy images of L929 cells after 24 h of treatment with (a)–(d) bare BG and (e)–(h) PDLLA-grafted BG samples, following live/dead staining. The positive control (TCPS) is shown at the bottom (scale bar = 180 μm). Green fluorescence corresponds to viable cells with intact membranes, while red fluorescence indicates dead cells with compromised plasma membranes.

Cu-doped MPs, while ternary (non-doped) MPs aggregates appear light grey. These observations are consistent with the MTS assay results, confirming a dose-dependent cytotoxic effect with increasing Cu content, as indicated by the decreasing cell density. In contrast, PDLLA-grafted BG samples did not display the same cytotoxic behaviour; even PDLLA-BG5 maintained a significantly higher cell density after 24 h of contact with L929. It should be noted, however, that Brightfield microscopy alone cannot distinguish living from dead cells. Therefore, a live/dead fluorescence assay was performed. Fluorescence microscopy images of L929 cells treated for 24 h with bare BG (Fig. 8a–d) and PDLLA-grafted BG (Fig. 8e–h) are shown. For the same reasons mentioned above, images of L929 cells after 48 h and of MC3T3-E1 cells at both 24 and 48 h are not reported.

The live cell dye (calcein AM) stains intact and viable cells in green. It is membrane-permeant and non-fluorescent until intracellular esterases cleave its ester groups, thereby producing a fluorescent molecule. Its maximum excitation and emission wavelengths are λ_{exc} = 494 nm and λ_{em} = 515 nm, respectively (similar to FITC). The dead cell dye (ethidium homodimer-1) labels cells with compromised plasma membranes in red. Being membrane-impermeant, it binds to DNA with high affinity and exhibits a >30-fold increase in fluorescence upon binding. Its maximum excitation and emission wavelengths are λ_{exc} = 528 nm and λ_{em} = 617 nm, respectively.

Fluorescence imaging further corroborates the results of the MTS assay and brightfield microscopy. The number of dead cells increases with higher Cu content, whereas the presence of the polyester corona appears to mitigate the cytotoxic effect, even at the highest Cu levels. This protective effect is attributed to the grafted polyester corona, which delays Cu release during the early hours of immersion. Such a delay is crucial, as the rapid release of Cu^{2+} ions is primarily responsible for cell death through the abrupt increase of intracellular ROS production triggered by ion uptake. As discussed in the previous section, this delay can be also extended or reduced by adjusting the Cu^{2+}/Cu^{0} ratio, *e.g.* delay increased by increasing the amount of Cu^{0} NPs.

4. Conclusion

This research work aimed, for the first time, to develop core–shell structures composed of copper-doped ternary bioactive glass microparticles and poly(D,L-lactide) *via* a grafting from approach. The four glasses selected were quaternary bioactive glass microparticles whose synthesis feasibility was demonstrated in a recent study by combining spray-drying with sol–gel chemistry, with copper contents ranging from 0 to 5 at%. These PDLLA-grafted particles were designed to be used as "building blocks" for the fabrication of composite scaffolds by freeze casting. In addition to their primary role in ensuring the mechanical cohesion of the final scaffolds, grafting was intended to improve the colloidal stability of micron-sized bioactive glasses in free PDLLA/dimethyl carbonate solutions. Indeed, due to the low affinity of BG for free polymer chains and the organic solvent, combined with the predominance of gravitational forces, the inorganic particles tend to precipitate during the freeze-casting process. To overcome this, surface-initiated ring-opening polymerisation of D,L-lactide was successfully carried out from the surface of amino-functionalised BG powders, as demonstrated by the FT-IR detection of amide bond vibrations. Furthermore, the polymer grafting density and the molecular weights of the grafted chains were estimated by TGA analysis, yielding satisfactory results, particularly with respect to chain lengths, which were very close to the theoretical values.

During this grafting from approach, the occurrence of free polymer chains in solution was observed, probably initiated by polar impurities or traces of moisture. With better control of the ROP process – for instance, by adding free initiators – the presence of well-defined free polymer chains could be exploited to fabricate composite scaffolds without the need to add additional free PDLLA chains, thereby turning a drawback into an opportunity to simplify the synthesis steps. Beyond the proof of concept demonstrated in the present work, the grafting density and yield of grafted chains can be further optimised through different strategies, such as the use of more reactive surface initiators, more accurate characterisation, and optimisation of the monomer-to-initiator ratio. This potential makes the grafting from strategy highly promising for the synthesis of well-defined core–shell structures.

Acellular degradation tests in SBF were performed on PDLLA-grafted BG samples and compared with those of the as-synthesised bare powders, with the aim of investigating the influence of the grafted polymer corona on the kinetics of ion release and the amount of nanocrystalline apatite formed. The results confirmed that the hybrid MPs were also bioactive, forming a hydroxyapatite layer on the glass surface. Interestingly, the presence of a polymer shell, owing to its hydrophobic nature and to medium buffering by acidic degradation products, induced a temporary shielding effect on the BG samples, thereby reducing the effective surface area available for ionic exchange. This slowed down ion diffusion into the medium, attenuating the burst effect, particularly for copper ions release.

Finally, the *in vitro* biological assessment of both PDLLA-grafted and bare BG samples was performed, evaluating the antibacterial potential of the recovered SBF solutions against *E. coli* and the cell viability for particles in direct contact with murine fibroblasts and an osteoblastic cell line. All samples exhibited a dose-dependent antibacterial and cytotoxic effect, which increased with the Cu content in the MPs. The best compromise between cytocompatibility and antibacterial performance was found in PDLLA-BG5, whose polyester corona delayed Cu^{2+} release and thus reduced the extent of the burst effect. Consequently, a lower initial release but more sustained over time ensured good *in vitro* cytocompatibility without compromising antibacterial activity. In this context, the *in vitro* biological properties can be modulated by controlling both the amount and the release kinetics of copper. Two main levers can be activated to achieve a prolonged and effective release: (i) the formulation of the bioactive glass, particularly by tuning the Cu-doping amount et more precisely, the Cu^{2+}/Cu^{0} ratio, and (ii) the presence of PDLLA chains, whose hydrophobic character, together with the acidity resulting from their hydrolytic degradation, may directly or indirectly influence the final biological properties. In conclusion, the versatility of these synthesised systems constitutes a promising way to potentially control the cytocompatibility and antibacterial activity depending on the application.

In conclusion, the versatility of this synthesis strategy offers a promising approach to control cytocompatibility and antibacterial activity at the scale of organic/inorganic particles, and will help to better understand and tailor the properties of scaffolds fabricated from these building blocks.

Author contributions

Gabriele Vecchio: data curation, formal analysis, investigation, methodology, writing – original draft. Vincent Darcos: funding acquisition, methodology, project administration, writing – original draft, writing – review & editing. Christèle Combes: methodology, validation, writing – review & editing David Bertrand: investigation, writing – review & editing. Audrey Béthry: methodology, investigation, formal analysis, validation, writing – review & editing. Marie-Pierre Castanié-Cornet: investigation, formal analysis, methodology, validation, writing – review & editing. Valentine Poissonnet: investigation, methodology, writing – review & editing. Agnès Dupret-Bories: funding acquisition, project administration, validation, writing – review & editing. Fabien Brouillet: methodology, validation, writing – review & editing. Sylvain Le Grill: methodology, validation, writing – review & editing. Jérémy Soulié: funding acquisition, methodology, project administration, writing – original draft, writing – review & editing, corresponding author.

Conflicts of interest

The authors declare that they have no known competing financial interests or personal relationships that could have appeared to influence the work reported in this paper.

Data availability

The data supporting the findings of this study are available within the article and its supplementary information (SI). The supplementary information includes evaluation of primary amines grafted onto the microsphere surface; polymerization conditions and determination of theoretical molecular weights; evaluation of PDLLA grafting density and molecular weight of the grafted chains; additional experimental results complementing those presented in the main article. See DOI: https://doi.org/10.1039/d5tb02273h.

Acknowledgements

The authors thank the French National Research Agency for funding (CongOs project: ANR-20-CE19-0019), Yannick Thebault (CIRIMAT) for EDX analysis, and Claire Fonquernie (Laboratoire Magma et Volcan, Clermont Ferrand, France) for ICP-OES measurements. We would like to thank the SynBio3 platform (IBMM, UMR 5247 Montpellier) for SEC and TGA analysis, whose equipment was publicly funded through the I-SITE Excellence Program of the University of Montpellier, under the "Investissements France 2030". During the preparation of this work, the authors used ChatGPT-5 to improve the English language and style. After using this tool, the authors

carefully reviewed and edited the content as needed and take full responsibility for the final version of the manuscript.

References

1 S. T. Kao and D. D. Scott, A Review of Bone Substitutes, *Oral Maxillofac. Surg. Clin. N. Am.*, 2007, **19**, 513–521, DOI: 10.1016/j.coms.2007.06.002.
2 P. V. Giannoudis, H. Dinopoulos and E. Tsiridis, Bone substitutes: An update, *Injury*, 2005, **36**, S20–S27, DOI: 10.1016/j.injury.2005.07.029.
3 T. Albrektsson and C. Johansson, Osteoinduction, osteoconduction and osseointegration, *Eur. Spine J.*, 2001, **10**, S96–S101, DOI: 10.1007/s005860100282.
4 L. Polo-Corrales, M. Latorre-Esteves and J. E. Ramirez-Vick, Scaffold Design for Bone Regeneration, *J. Nanosci. Nanotechnol.*, 2014, **14**, 15–56, DOI: 10.1166/jnn.2014.9127.
5 P. D. Costantino and C. D. Friedman, Synthetic Bone Graft Substitutes, *Otolaryngol. Clin. N. Am.*, 1994, **27**, 1037–1074, DOI: 10.1016/S0030-6665(20)30622-8.
6 N. Rice, I. Polyzois, K. Ekanayake, O. Omer and L. F. A. Stassen, The management of osteoradionecrosis of the jaws – A review, *Surgeon*, 2015, **13**, 101–109, DOI: 10.1016/j.surge.2014.07.003.
7 P. Lagarrigue, J. Soulié, E. Chabrillac, V. Darcos, D. Grossin, S. Vergez, C. Combes and A. Dupret-Bories, Biomaterials and osteoradionecrosis of the jaw: Review of the literature according to the SWiM methodology, *Eur. Ann. Otorhinolaryngol. Head Neck Dis.*, 2022, **139**, 208–215, DOI: 10.1016/j.anorl.2021.06.006.
8 L. L. Hench, R. J. Splinter, W. C. Allen and T. K. Greenlee, Bonding mechanisms at the interface of ceramic prosthetic materials, *J. Biomed. Mater. Res.*, 1971, **5**, 117–141, DOI: 10.1002/jbm.820050611.
9 L. L. Hench, The story of Bioglass®, *J. Mater. Sci.: Mater. Med.*, 2006, **17**, 967–978, DOI: 10.1007/s10856-006-0432-z.
10 J. R. Jones, Review of bioactive glass: From Hench to hybrids, *Acta Biomater.*, 2013, **9**, 4457–4486, DOI: 10.1016/j.actbio.2012.08.023.
11 D. S. Brauer, Bioactive Glasses—Structure and Properties, *Angew. Chem., Int. Ed.*, 2015, **54**, 4160–4181, DOI: 10.1002/anie.201405310.
12 H. Palza, B. Escobar, J. Bejarano, D. Bravo, M. Diaz-Dosque and J. Perez, Designing antimicrobial bioactive glass materials with embedded metal ions synthesized by the sol–gel method, *Materials Science and Engineering: C*, 2013, **33**, 3795–3801, DOI: 10.1016/j.msec.2013.05.012.
13 L. R. Rivera, A. Cochis, S. Biser, E. Canciani, S. Ferraris, L. Rimondini and A. R. Boccaccini, Antibacterial, pro-angiogenic and pro-osteointegrative zein-bioactive glass/copper based coatings for implantable stainless steel aimed at bone healing, *Bioactive Materials*, 2021, **6**, 1479–1490, DOI: 10.1016/j.bioactmat.2020.11.001.
14 A. Braem, N. H. N. Kamarudin, N. Bhaskar, Z. Hadzhieva, A. Mele, J. Soulié, D. P. Linklater, L. Bonilla-Gameros, A. R. Boccaccini, I. Roy, C. Drouet, E. P. Ivanova, D. Mantovani and B. Basu, Biomaterial strategies to combat implant infections: new perspectives to old challenges, *Int. Mater. Rev.*, 2023, 1–39, DOI: 10.1080/09506608.2023.2193784.
15 J. V. Rau, M. Curcio, M. G. Raucci, K. Barbaro, I. Fasolino, R. Teghil, L. Ambrosio, A. De Bonis and A. R. Boccaccini, Cu-Releasing Bioactive Glass Coatings and Their in Vitro Properties, *ACS Appl. Mater. Interfaces*, 2019, **11**, 5812–5820, DOI: 10.1021/acsami.8b19082.
16 Z. Lin, Y. Cao, J. Zou, F. Zhu, Y. Gao, X. Zheng, H. Wang, T. Zhang and T. Wu, Improved osteogenesis and angiogenesis of a novel copper ions doped calcium phosphate cement, *Mater. Sci. Eng., C*, 2020, **114**, 111032, DOI: 10.1016/j.msec.2020.111032.
17 J. Barralet, U. Gbureck, P. Habibovic, E. Vorndran, C. Gerard and C. J. Doillon, Angiogenesis in Calcium Phosphate Scaffolds by Inorganic Copper Ion Release, *Tissue Eng., Part A*, 2009, **15**, 1601–1609, DOI: 10.1089/ten.tea.2007.0370.
18 A. Hoppe, N. S. Güldal and A. R. Boccaccini, A review of the biological response to ionic dissolution products from bioactive glasses and glass-ceramics, *Biomaterials*, 2011, **32**, 2757–2774, DOI: 10.1016/j.biomaterials.2011.01.004.
19 Z. L. Sun, J. C. Wataha and C. T. Hanks, Effects of metal ions on osteoblast-like cell metabolism and differentiation, *J. Biomed. Mater. Res.*, 1997, **34**, 29–37, DOI: 10.1002/(SICI)1097-4636(199701)34:1%253C29::AID-JBM5%253E3.0.CO;2-P.
20 I. Cacciotti, Bivalent cationic ions doped bioactive glasses: the influence of magnesium, zinc, strontium and copper on the physical and biological properties, *J. Mater. Sci.*, 2017, **52**, 8812–8831, DOI: 10.1007/s10853-017-1010-0.
21 A. R. Boccaccini, M. Erol, W. J. Stark, D. Mohn, Z. Hong and J. F. Mano, Polymer/bioactive glass nanocomposites for biomedical applications: A review, *Compos. Sci. Technol.*, 2010, **70**, 1764–1776, DOI: 10.1016/j.compscitech.2010.06.002.
22 D. Garlotta, A literature review of poly (lactic acid), *J. Polym. Environ.*, 2001, **9**, 63–84.
23 S. Farah, D. G. Anderson and R. Langer, Physical and mechanical properties of PLA, and their functions in widespread applications—A comprehensive review, *Adv. Drug Delivery Rev.*, 2016, **107**, 367–392, DOI: 10.1016/j.addr.2016.06.012.
24 N.-A. A. B. Taib, M. R. Rahman, D. Huda, K. K. Kuok, S. Hamdan, M. K. B. Bakri, M. R. M. B. Julaihi and A. Khan, A review on poly lactic acid (PLA) as a biodegradable polymer, *Polym. Bull.*, 2023, **80**, 1179–1213, DOI: 10.1007/s00289-022-04160-y.
25 R. Auras, B. Harte and S. Selke, An Overview of Polylactides as Packaging Materials, *Macromol. Biosci.*, 2004, **4**, 835–864, DOI: 10.1002/mabi.200400043.
26 J. Coudane, H. Van Den Berghe, J. Mouton, X. Garric and B. Nottelet, Poly(Lactic Acid)-Based Graft Copolymers: Syntheses Strategies and Improvement of Properties for Biomedical and Environmentally Friendly Applications: A Review, *Molecules*, 2022, **27**, 4135, DOI: 10.3390/molecules27134135.

27 T. Jiang, E. J. Carbone, K. W.-H. Lo and C. T. Laurencin, Electrospinning of polymer nanofibers for tissue regeneration, *Prog. Polym. Sci.*, 2015, **46**, 1–24, DOI: 10.1016/j.progpolymsci.2014.12.001.
28 F. Álvarez-Carrasco, P. Varela, M. A. Sarabia-Vallejos, C. García-Herrera, M. Saavedra, P. A. Zapata, D. Zárate-Triviño, J. J. Martínez and D. A. Canales, Development of Bioactive Hybrid Poly(lactic acid)/Poly(methyl methacrylate) (PLA/PMMA) Electrospun Fibers Functionalized with Bioglass Nanoparticles for Bone Tissue Engineering Applications, *IJMS*, 2024, **25**, 6843, DOI: 10.3390/ijms25136843.
29 A. Prasad, M. R. Sankar and V. Katiyar, State of Art on Solvent Casting Particulate Leaching Method for Orthopedic ScaffoldsFabrication, *Mater. Today: Proc.*, 2017, **4**, 898–907, DOI: 10.1016/j.matpr.2017.01.101.
30 N. Thadavirul, P. Pavasant and P. Supaphol, Development of polycaprolactone porous scaffolds by combining solvent casting, particulate leaching, and polymer leaching techniques for bone tissue engineering, *J. Biomed. Mater. Res.*, 2014, **102**, 3379–3392, DOI: 10.1002/jbm.a.35010.
31 D. von Heimburg, S. Zachariah, H. Kühling, I. Heschel, H. Schoof, B. Hafemann and N. Pallua, Human preadipocytes seeded on freeze-dried collagen scaffolds investigated in vitro and in vivo, *Biomaterials*, 2001, **22**, 429–438.
32 F. Asghari, M. Samiei, K. Adibkia, A. Akbarzadeh and S. Davaran, Biodegradable and biocompatible polymers for tissue engineering application: a review, *Artif. Cells, Nanomed., Biotechnol.*, 2017, **45**, 185–192, DOI: 10.3109/21691401.2016.1146731.
33 Y. Liu, J. Lim and S.-H. Teoh, Review: Development of clinically relevant scaffolds for vascularised bone tissue engineering, *Biotechnol. Adv.*, 2013, **31**, 688–705, DOI: 10.1016/j.biotechadv.2012.10.003.
34 C. Shuai, W. Yang, P. Feng, S. Peng and H. Pan, Accelerated degradation of HAP/PLLA bone scaffold by PGA blending facilitates bioactivity and osteoconductivity, *Bioact. Mater.*, 2021, **6**, 490–502, DOI: 10.1016/j.bioactmat.2020.09.001.
35 P. Feng, P. Wu, C. Gao, Y. Yang, W. Guo, W. Yang and C. Shuai, A Multimaterial Scaffold With Tunable Properties: Toward Bone Tissue Repair, *Adv. Sci.*, 2018, **5**, 1700817, DOI: 10.1002/advs.201700817.
36 C. Shuai, Z. Wang, H. Zhang, J. Jia, L. Huang, D. Wang, S. Chen and P. Feng, Biosoluble ceramic fiber reinforced poly(L-lactic acid) bone scaffold: degradation and bioactivity, *Npj Mater. Degrad.*, 2022, **6**, 87, DOI: 10.1038/s41529-022-00297-3.
37 J. Esmaeilzadeh, S. Hesaraki, S. M.-M. Hadavi, M. H. Ebrahimzadeh and M. Esfandeh, Poly (D/L) lactide/polycaprolactone/bioactive glasss nanocomposites materials for anterior cruciate ligament reconstruction screws: The effect of glass surface functionalization on mechanical properties and cell behaviors, *Mater. Sci. Eng., C*, 2017, **77**, 978–989, DOI: 10.1016/j.msec.2017.03.134.
38 R. Odermatt, M. Par, D. Mohn, D. B. Wiedemeier, T. Attin and T. T. Tauböck, Bioactivity and Physico-Chemical Properties of Dental Composites Functionalized with Nano- vs. Micro-Sized Bioactive Glass, *JCM*, 2020, **9**, 772, DOI: 10.3390/jcm9030772.
39 T. S. Petrovskaya, N. E. Toropkov and A. N. Fomenko, Evaluation of the Bioactive Properties of the Mineral-Polymer Composite Calcium Phosphates – Polylactide, *Glass Ceram.*, 2021, **78**, 317–322, DOI: 10.1007/s10717-021-00402-z.
40 Z. Hong, R. L. Reis and J. F. Mano, Preparation and in vitro characterization of scaffolds of poly(l-lactic acid) containing bioactive glass ceramic nanoparticles, *Acta Biomater.*, 2008, **4**, 1297–1306, DOI: 10.1016/j.actbio.2008.03.007.
41 N. Jain, J. Schmidt, O. Görke, D. Karl, A. Gurlo and F. Schmidt, Surface modification of bioactive glasses for successful incorporation with poly(lactic- *co* -glycolic acid) (PLGA), *Appl. Interfaces*, 2024, **1**, 748–758, DOI: 10.1039/D3LF00273J.
42 W. R. Lenart and M. J. A. Hore, Structure–property relationships of polymer-grafted nanospheres for designing advanced nanocomposites, *Nano-Struct. Nano-Objects*, 2018, **16**, 428–440, DOI: 10.1016/j.nanoso.2017.11.005.
43 R. A. E. Wright, K. Wang, J. Qu and B. Zhao, Oil-Soluble Polymer Brush Grafted Nanoparticles as Effective Lubricant Additives for Friction and Wear Reduction, *Angew. Chem.*, 2016, **128**, 8798–8802, DOI: 10.1002/ange.201603663.
44 P. Lagarrigue, J. Soulié, D. Grossin, A. Dupret-Bories, C. Combes and V. Darcos, Well-defined polyester-grafted silica nanoparticles for biomedical applications: Synthesis and quantitative characterization, *Polymer*, 2020, **211**, 123048, DOI: 10.1016/j.polymer.2020.123048.
45 A. J. Chancellor, B. T. Seymour and B. Zhao, Characterizing Polymer-Grafted Nanoparticles: From Basic Defining Parameters to Behavior in Solvents and Self-Assembled Structures, *Anal. Chem.*, 2019, **91**, 6391–6402, DOI: 10.1021/acs.analchem.9b00707.
46 F. Wu, B. Zhang, W. Yang, Z. Liu and M. Yang, Inorganic silica functionalized with PLLA chains via grafting methods to enhance the melt strength of PLLA/silica nanocomposites, *Polymer*, 2014, **55**, 5760–5772, DOI: 10.1016/j.polymer.2014.08.070.
47 D.-W. Shi, X.-L. Lai, Y.-P. Jiang, C. Yan, Z.-Y. Liu, W. Yang and M.-B. Yang, Synthesis of Inorganic Silica Grafted Three-arm PLLA and Their Behaviors for PLA Matrix, *Chin. J. Polym. Sci.*, 2019, **37**, 216–226, DOI: 10.1007/s10118-019-2191-6.
48 M. Klein Gunnewiek, A. Di Luca, X. Sui, C. A. van Blitterswijk, L. Moroni and G. J. Vancso, Controlled Surface Initiated Polymerization of *N* -Isopropylacrylamide from Polycaprolactone Substrates for Regulating Cell Attachment and Detachment, *Isr. J. Chem.*, 2012, **52**, 339–346, DOI: 10.1002/ijch.201100118.
49 L. Chang, H. Yan, J. Chang and J. E. Gautrot, Cationic polymer brush-coated bioglass nanoparticles for the design of bioresorbable RNA delivery vectors, *Eur. Polym. J.*, 2021, **156**, 110593, DOI: 10.1016/j.eurpolymj.2021.110593.
50 H. Takahashi, M. Nakayama, M. Yamato and T. Okano, Controlled Chain Length and Graft Density of Thermoresponsive Polymer Brushes for Optimizing Cell Sheet

Harvest, *Biomacromolecules*, 2010, **11**, 1991–1999, DOI: 10.1021/bm100342e.

51 T. Zhu, M. A. Rahman and B. C. Benicewicz, Synthesis of Well-Defined Polyolefin Grafted SiO_2 Nanoparticles with Molecular Weight and Graft Density Control, *ACS Macro Lett.*, 2020, **9**, 1255–1260, DOI: 10.1021/acsmacrolett.0c00398.

52 T. Hao, Y. Wang, Z. Liu, J. Li, L. Shan, W. Wang, J. Liu and J. Tang, Emerging Applications of Silica Nanoparticles as Multifunctional Modifiers for High Performance Polyester Composites, *Nanomaterials*, 2021, **11**, 2810, DOI: 10.3390/nano11112810.

53 X. Wen, One-pot route to graft long-chain polymer onto silica nanoparticles and its application for high-performance poly(L -lactide) nanocomposites, *RSC Adv.*, 2019, **9**, 13908–13915, DOI: 10.1039/C9RA01360A.

54 M. Husseman, E. E. Malmström, M. McNamara, M. Mate, D. Mecerreyes, D. G. Benoit, J. L. Hedrick, P. Mansky, E. Huang, T. P. Russell and C. J. Hawker, Controlled Synthesis of Polymer Brushes by ''Living'' Free Radical Polymerization Techniques, *Macromolecules*, 1999, **32**, 1424–1431, DOI: 10.1021/ma981290v.

55 D. Li, X. Sheng and B. Zhao, Environmentally Responsive ''Hairy'' Nanoparticles: Mixed Homopolymer Brushes on Silica Nanoparticles Synthesized by Living Radical Polymerization Techniques, *J. Am. Chem. Soc.*, 2005, **127**, 6248–6256, DOI: 10.1021/ja0422561.

56 K. Ohno, K. Koh, Y. Tsujii and T. Fukuda, Fabrication of Ordered Arrays of Gold Nanoparticles Coated with High-Density Polymer Brushes, *Angew. Chem., Int. Ed.*, 2003, **42**, 2751–2754, DOI: 10.1002/anie.200250850.

57 M. Chen, Y. Wang, P. Yuan, L. Wang, X. Li and B. Lei, Multifunctional bioactive glass nanoparticles: surface–interface decoration and biomedical applications, *Regener. Biomater.*, 2024, **11**, rbae110, DOI: 10.1093/rb/rbae110.

58 J. Bejarano, A. R. Boccaccini, C. Covarrubias and H. Palza, Effect of Cu- and Zn-Doped Bioactive Glasses on the In Vitro Bioactivity, Mechanical and Degradation Behavior of Biodegradable PDLLA Scaffolds, *Materials*, 2020, **13**, 2908, DOI: 10.3390/ma13132908.

59 J. Bejarano, R. Detsch, A. R. Boccaccini and H. Palza, PDLLA scaffolds with Cu- and Zn-doped bioactive glasses having multifunctional properties for bone regeneration, *J. Biomed. Mater. Res., Part A*, 2017, **105**, 746–756, DOI: 10.1002/jbm.a.35952.

60 G. Vecchio, V. Darcos, S. L. Grill, F. Brouillet, Y. Coppel, M. Duttine, A. Pugliara, C. Combes and J. Soulié, Spray-dried ternary bioactive glass microspheres: Direct and indirect structural effects of copper-doping on acellular degradation behavior, *Acta Biomater.*, 2024, **181**, 453–468, DOI: 10.1016/j.actbio.2024.05.003.

61 M. Joubert, C. Delaite, E. Bourgeat Lami and P. Dumas, Synthesis of poly(ε-caprolactone)–silica nanocomposites: from hairy colloids to core–shell nanoparticles, *New J. Chem.*, 2005, **29**, 1601, DOI: 10.1039/b508649c.

62 E. San Andrés, A. Del Prado, I. Mártil, G. González-Diaz, D. Bravo, F. J. López, M. Fernández, W. Bohne, J. Röhrich, B. Selle and I. Sieber, Bonding configuration and density of defects of SiO[sub x]H[sub y] thin films deposited by the electron cyclotron resonance plasma method, *J. Appl. Phys.*, 2003, **94**, 7462, DOI: 10.1063/1.1626798.

63 I. A. Rahman, P. Vejayakumaran, C. S. Sipaut, J. Ismail and C. K. Chee, Size-dependent physicochemical and optical properties of silica nanoparticles, *Mater. Chem. Phys.*, 2009, **114**, 328–332, DOI: 10.1016/j.matchemphys.2008.09.068.

64 S. Rovani, J. Santos, P. Corio and D. Fungaro, An Alternative and Simple Method for the Preparation of Bare Silica Nanoparticles Using Sugarcane Waste Ash, an Abundant and Despised Residue in the Brazilian Industry, *J. Braz. Chem. Soc.*, 2019, **30**, 1524–1533.

65 N. Vandecandelaere, C. Rey and C. Drouet, Biomimetic apatite-based biomaterials: on the critical impact of synthesis and post-synthesis parameters, *J. Mater. Sci.: Mater. Med.*, 2012, **23**, 2593–2606, DOI: 10.1007/s10856-012-4719-y.

66 S. Akhtach, Z. Tabia, K. El Mabrouk, M. Bricha and R. Belkhou, A comprehensive study on copper incorporated bio-glass matrix for its potential antimicrobial applications, *Ceram. Int.*, 2021, **47**, 424–433, DOI: 10.1016/j.ceramint.2020.08.149.

67 F. Errassifi, S. Sarda, A. Barroug, A. Legrouri, H. Sfihi and C. Rey, Infrared, Raman and NMR investigations of risedronate adsorption on nanocrystalline apatites, *J. Colloid Interface Sci.*, 2014, **420**, 101–111, DOI: 10.1016/j.jcis.2014.01.017.

68 B. Smith, Organic Nitrogen Compounds, VII: Amides—The Rest of the Story, *Spectroscopy*, 2020, **35**, 10–15.

69 F. Wu, X. Lan, D. Ji, Z. Liu, W. Yang and M. Yang, Grafting polymerization of polylactic acid on the surface of nano-SiO2 and properties of PLA/PLA-grafted-SiO2 nanocomposites, *J. Appl. Polym. Sci.*, 2013, **129**, 3019–3027, DOI: 10.1002/app.38585.

70 R. Mueller, H. K. Kammler, K. Wegner and S. E. Pratsinis, OH Surface Density of SiO_2 and TiO_2 by Thermogravimetric Analysis, *Langmuir*, 2003, **19**, 160–165, DOI: 10.1021/la025785w.

71 A. El-Fiqi, T.-H. Kim, M. Kim, M. Eltohamy, J.-E. Won, E.-J. Lee and H.-W. Kim, Capacity of mesoporous bioactive glass nanoparticles to deliver therapeutic molecules, *Nanoscale*, 2012, **4**, 7475, DOI: 10.1039/c2nr31775c.

72 M. C. Chang and J. Tanaka, FT-IR study for hydroxyapatite/collagen nanocomposite cross-linked by glutaraldehyde, *Biomaterials*, 2002, **23**, 4811–4818, DOI: 10.1016/S0142-9612(02)00232-6.

73 J. Xu and D. Xue, Fabrication of Copper Hydroxyphosphate with Complex Architectures, *J. Phys. Chem. B*, 2006, **110**, 7750–7756, DOI: 10.1021/jp0574448.

74 Y. Zhan, H. Li and Y. Chen, Copper hydroxyphosphate as catalyst for the wet hydrogen peroxide oxidation of azo dyes, *J. Hazard. Mater.*, 2010, **180**, 481–485, DOI: 10.1016/j.jhazmat.2010.04.055.

75 M. C. Cortizo and M. F. L. De Mele, Cytotoxicity of Copper Ions Released from Metal: Variation with the Exposure

Period and Concentration Gradients, *BTER*, 2004, **102**, 129–142, DOI: 10.1385/BTER:102:1-3:129.

76 A. M. Studer, L. K. Limbach, L. Van Duc, F. Krumeich, E. K. Athanassiou, L. C. Gerber, H. Moch and W. J. Stark, Nanoparticle cytotoxicity depends on intracellular solubility: Comparison of stabilized copper metal and degradable copper oxide nanoparticles, *Toxicol. Lett.*, 2010, **197**, 169–174, DOI: 10.1016/j.toxlet.2010.05.012.